# Susceptibility of a mesoscopic superconducting ring

Xiaxian Zhang and John C. Price
*Department of Physics, University of Colorado, Boulder, Colorado 80309*
(Received 19 August 1996)

The susceptibility of a single mesoscopic aluminum ring has been studied with an integrated superconducting quantum interference device susceptometer at temperatures near the superconducting critical temperature, and anomalous behavior has been found just above $T_c$. Below the zero-field critical temperature of 1.266 K we find excellent agreement with a Ginzburg-Landau theory of the susceptibility, and all of the important sample parameters can be accurately determined. The phase-slip transition rates are measured as a function of flux at temperatures down to 0.950 K, and a comparison with the theoretical free-energy barrier heights for these transitions shows that we are able to predict the ratio of the saddle-point energy to the initial-state energy with an accuracy of a few percent. Just above the mean-field $T_c$ we expect the susceptibility to be dominated by thermodynamic fluctuations. A clear signal is found from $T_c$ to 25 mK above $T_c$, but it is as much as 50 times larger than predicted. The observed phase-slip rates can be used to show that this anomalously large susceptibility just above $T_c$ is not due to temperature fluctuations and that it is not a noise-driven effect. [S0163-1829(97)02505-8]

## I. INTRODUCTION

Experiments on small superconducting rings and cylinders have provided clear demonstrations of many features of superconductivity. Phenomena studied by susceptibility or inductive coupling experiments include the original demonstrations of flux quantization,[1] the thermal decay of supercurrents in rings containing weak links,[2] the current-phase relationship for weak links,[3] and macroscopic quantum effects.[4] Transport measurements on rings and cylinders have addressed the Little-Parks $T_c$ oscillations,[5,6] and magnetoconductance oscillations due to superconducting fluctuations.[7] Recently, transport experiments involving mesoscopic superconducting rings ($\approx 1$ $\mu$m diameter) have explored the locality of fluctuation effects,[8] and the influence of a superconducting boundary on quantum transport.[9] In the present work we extend the scope of susceptibility measurements to single mesoscopic superconducting rings. We use the susceptibility and phase-slip rate below $T_c$ to characterize the ring in terms of Ginzburg-Landau theory, and then show that the susceptibility above $T_c$ is anomalously large. Davidovic *et al.*[10] have described experiments on the susceptibility of rings very similar to ours, but in large arrays. That work focuses on the effects of interactions between rings, while we attempt to understand the detailed behavior of a single ring.

What new features might be revealed in the susceptibility of mesoscopic superconducting rings? One of the initial motivations for our experiments was an interest in mesoscopic effects in the sense of quantum transport physics. The distinguishing feature of such effects is that they are sample specific in macroscopically identical samples because they depend on the detailed configuration of the microscopic disorder. In rings, mesoscopic effects arise from the $h/e$-period flux dependence of the single-electron energy levels. An $h/e$-periodic contribution to the susceptibility of a small ballistic superconducting ring was suggested long ago by Bogacheck, Gogadze, and Kulik.[11] In normal-metal and semiconducting mesoscopic rings $h/e$-periodic persistent currents have recently been observed.[12] Conductance oscillations with period $h/e$ are established in transport experiments on mesoscopic rings.[13] However, no $h/e$-periodic effects were visible in the experiments reported here. Such effects may yet be observed in smaller samples or in samples with lower critical temperatures.

Besides sample-specific mesoscopic effects, small samples with low $T_c$ are distinguished by the importance of thermodynamic fluctuation effects, due to the small condensation energy, which is proportional to the sample volume and to the square of the critical temperature. Two types of thermodynamic fluctuation phenomena may be distinguished: small fluctuations about an equilibrium configuration which is a local minimum of the Ginzburg-Landau free energy, and large fluctuations which cause transitions between different local minima.[14]

Large fluctuations occur via localized phase slips of the order parameter in samples which are one-dimensional with respect to the Ginzburg-Landau coherence length.[15] The phase-slip rate has been studied previously by measuring the resistance of fine wires[16] very close to the mean-field $T_c$, and phase slips have also been studied by susceptibility in rings containing weak links.[2] It appears that phase slips have not been studied before in homogeneous one-dimensional rings by susceptibility. Such experiments are attractive because, rather than measuring an average rate, one may observe single phase-slip events between distinct initial and final states, and much lower phase-slip rates can be studied than is possible in transport. It is also possible to observe effects which only appear when the circumference is comparable to the Ginzburg-Landau coherence length. We measure the phase-slip rate as a function of both temperature and flux, and compare our measurements to a calculation which predicts the free-energy barrier height.

The small fluctuations lead to a contribution to the susceptibility which is nonzero above the mean-field $T_c$. In small samples this fluctuation susceptibility has been studied previously in a collection of fine aluminum particles with a

 

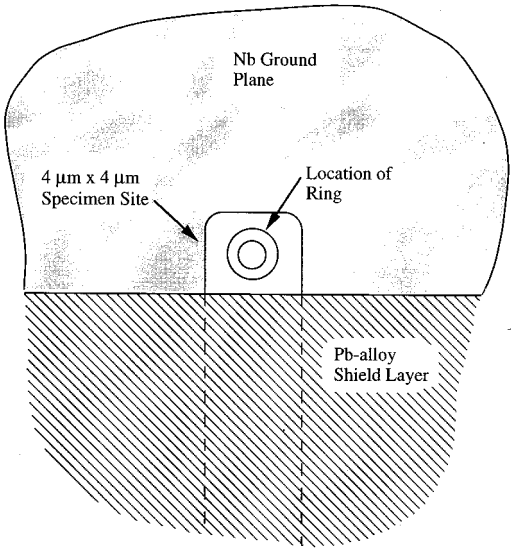


FIG. 1. The 4 $\mu$m by 4 $\mu$m specimen site on the susceptometer device. The lower Nb film is separated from the upper Pb-alloy film an SiO insulating layer.

known size distribution.[17] We report here a zero-field susceptibility just above $T_c$ which we find to be much too large to be explained by thermodynamic fluctuations of the Ginzburg-Landau free energy. We refer to this signal as the fluctuation susceptibility, although it may not in fact be a fluctuation effect. Hypotheses concerning the mechanism of this effect are highly constrained by our knowledge of the Ginzburg-Landau behavior and the phase-slip rates. Several conventional explanations for the signal are discussed and shown to be inadequate.

We begin in Sec. II below with a description of our microsusceptometer apparatus. The observed susceptibility in the absence of fluctuations is discussed in Sec. III, and a fit to Ginzburg-Landau theory is used to determine several sample parameters. We then discuss the phase slips in Sec. IV, and the fluctuation susceptibility in Sec. V. A circuit model of the susceptometer which has been used to evaluate the calibration constants is discussed in Appendix A, and Appendix B presents the theory of the phase-slip rate.

## II. APPARATUS AND SAMPLES

The three main components of our susceptometer system are a superconducting susceptometer device, a superconducting quantum interference device (SQUID) amplifier, and a small transparent sapphire substrate carrying the sample. The 100 $\mu$m$\times$2 mm$\times$2 mm sample substrate is glued to the top surface of the susceptometer chip. The sample ring is made by electron beam lithography on the lower surface of the sapphire sample substrate, and is aligned under an optical microscope with 0.5 $\mu$m accuracy to the sensitive specimen site on the susceptometer chip. This arrangement allows different samples and SQUID devices to be tested with the same susceptometer chip. In this section we discuss the susceptometer device and its calibration, the SQUID readout and other electronics, and the sample fabrication and mounting. A more detailed description of our apparatus and other

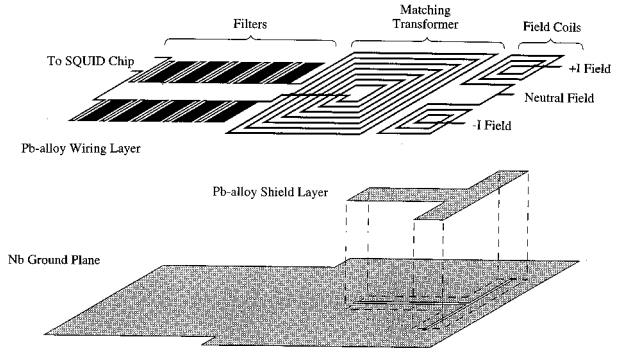


FIG. 2. Layout of the conducting layers of the susceptometer device. The ground plane is 4.4 mm long. The three layers shown are separated by SiO insulating layers. The upper Pb-alloy wiring is actually two layers as required to form the coil crossovers.

aspects of the experiments reported here is given elsewhere.[18]

The specimen site on the susceptometer chip is shown in Fig. 1. The susceptometer senses the change in inductance of a 4 $\mu$m$\times$4 $\mu$m square hole due to the presence of the sample ring. Three sides of the specimen site are formed by a 300 nm thick Nb ground plane film sputtered directly onto a sapphire substrate, and the fourth side is formed from an overlying 500 nm thick evaporated Pb-alloy (Pb-Au-In) film. The two superconducting films are separated by a 350 nm thick SiO insulating layer. Sapphire is chosen for the susceptometer substrate material to provide a thermal-expansion match to the sapphire sample substrate.

The physical layout of the conducting layers on the susceptometer chip is shown in Fig. 2, and a simplified schematic is shown in Fig. 3. The specimen site is connected in series with a second identical 4 $\mu$m square hole and a 12 $\mu$m square hole which forms the transformer primary. This series circuit is formed by a T-shaped slot in the Nb ground plane film. A wider T-shaped Pb-alloy film shields the inductance of the slot except at the ends. The three ends of the slot extend beyond the Pb-alloy shield and form the three holes.

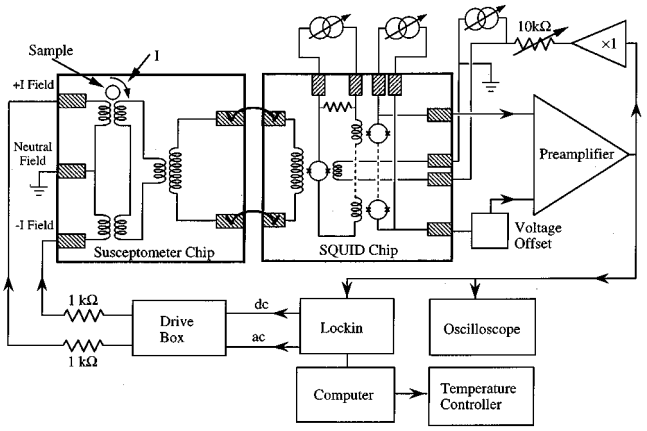


FIG. 3. Schematic of the experiment. The susceptometer device and SQUID amplifier are each fabricated on separate 6.2 mm square chips. The connection between these two devices is made by superconducting wire bonds. Only these two chips and the sample substrate are in the cryogenic environment.

The inductance of the primary circuit is matched to the 190 nH SQUID input inductance by a planar transformer.[19] The 76-turn transformer secondary is patterned in an upper Pb-alloy layer along with the two field coils and a pair of $LC$ ladder filters. The field coils are counter wound so that equal bias currents in the two field coils gives no signal at the SQUID in the absence of a sample. The $LC$ filters are provided to ensure that the sample is not heated by microwave-frequency flux from the SQUID's Josephson oscillations. The five-stage ladder filter has a cutoff frequency of 4 GHz and is designed to provide about 200 dB of attenuation at the $\approx$40 GHz Josephson frequency of the input SQUID.

The sample ring is fabricated on a separate 100 $\mu$m thick sapphire substrate by electron-beam lithography. This sapphire substrate is transparent and polished on both sides so that it can be aligned to the susceptometer chip under an optical microscope. The sample substrate is pushed into alignment using a fine needle connected to a precision three-axis translator mounted on the stage of the optical microscope. Once correctly located, the sample chip is held down with the needle and then glued in place with a drop of poly-(methyl methacrylate) (PMMA) electron-beam resist.

The sample patterning is done with a single-layer PMMA liftoff process. Because the substrate is an excellent insulator, the PMMA must be coated with 15 nm of aluminum before being exposed to the electron beam. This coating is etched away in a dilute NaOH solution before the PMMA is developed. After development, the sample chip is place in a bell-jar evaporator and exposed to an oxygen plasma for cleaning, and then the aluminum sample material is thermally evaporated. The final step is a liftoff in acetone with ultrasonic agitation.

The susceptometer chip with the sample and the SQUID chip are mounted on a copper-clad G-10 header which is bolted to a copper cold finger. Connections to the chips are made by three kinds of ultrasonic wire bonds. The SQUID input is connected to the susceptometer output with a Pb-alloy wire[20] that is superconducting at 4 K. Several gold wire bonds are used to connect large normal-metal pads on the SQUID chip to the copper header cladding for heat sinking. Aluminum wire bonds are used for other connections. The cold finger is enclosed in a thick niobium cylinder which shields against external magnetic fields.

Figure 3 shows the SQUID device and other electronics used in the experiments. The integrated SQUID amplifier chip was developed by Welty and Martinis.[21] A conventional voltage-biased input SQUID is followed by a 100 element series-array SQUID amplifier. This array provides sufficient gain so that no tank circuit or matching transformer is needed for coupling to the room-temperature JFET preamplifier (Stanford Research SR560). The input SQUID and SQUID array are biased to operate as linear amplifiers, and feedback is applied to the input SQUID to stabilize the overall gain. The noise of the SQUID system is about $1\mu\Phi_0/\mathrm{Hz}^{1/2}$ at 1 kHz, referred to the input SQUID loop. (We denote the quantum of flux as $\Phi_0 \equiv h/2e$.)

Data is collected by applying a small 1 kHz ac flux to the sample ring and detecting the output of the instrument at the same frequency with a lock-in amplifier. The data is thus proportional to the derivative of the circulating sample current with respect to the applied flux. The 1 kHz ac signal is generated by an oscillator in the lock-in and applied to the drive box, which generates balanced currents for the field coils. The drive box contains a gain trim in one channel which can be adjusted so the SQUID output signal is zero in the absence of the sample (or well above the sample critical temperature). A low-frequency sweep or dc signal is generated by the lock-in under computer control and summed with the ac signal in the drive box. This signal determines at what value of flux $\Phi$ the derivative signal $dI(\Phi)/d\Phi$ is measured.

Two calibration constants are needed to interpret the output of the instrument. We define these constants in such a way that they do not depend on whether or not we include the effects of the self-inductance of the sample ring or screening of the applied field by the ring. Because the experiments described here were done on small samples close to $T_c$, self-field effects do not play a major role.

If the data are expressed as a plot of $dI(\Phi)/d\Phi$ versus $\Phi$, the two calibration constants control the scaling of the $x$ and $y$ axes. The first determines the applied flux and is defined as the ratio of the flux applied to the sample ring to the balanced current applied to the field coils. The applied sample flux is taken as the total flux out to the mean radius of the sample, but in the absence of the sample. This quantity has the dimensions of an inductance and is denoted $M_{F\text{-}R}$ (field-to-ring). The periodicity in $\Phi_0$ of the induced sample current can be used to directly measure $M_{F\text{-}R}$. In the next section we give a Ginzburg-Landau model of the sample which predicts minima in $dI/d\Phi$ at the flux values

$$\Phi_n = \Phi_0 \frac{n}{1+(w/2R)^2}, \tag{1}$$

where $n$ is an integer. The denominator, which depends on the ratio of the ring linewidth $w$ to the mean radius $R$, shifts the minima by only 8%, and thus the locations of the minima can be predicted accurately even though $w$ is only known to 10%. This expression is exact to lowest order in $w/R$ and sufficiently close to $T_c$. For the data reported here we find $M_{F\text{-}R}^{-1} = 1130 \pm 11\ \mu\mathrm{A}/\Phi_0$.

The other calibration constant $M_{R\text{-}S}$ (ring-to-SQUID) determines the sample current. It is defined as the ratio of the flux induced in the input SQUID loop to the sample current, with zero field current. The sample current is taken to be an idealized line current at the mean radius of the sample. This constant cannot be directly measured. To avoid having the calibration depend on a large number of model parameters, some of which are not known accurately, it is helpful to express $M_{R\text{-}S}$ in terms of another quantity $M_{F\text{-}S}$ (field-to-SQUID), which can be directly measured. $M_{F\text{-}S}$ is the ratio of the SQUID flux to an unbalanced (single-sided) field coil current in the absence of a sample. A simple model of the system (see Appendix A) shows that

$$M_{R-S} = \frac{M_{F-R} M_{F-S}}{n_F M_F}. \tag{2}$$

Here $n_F = 10.75$ is the number of turns in one field coil and $M_F$ is the mutual inductance between one field coil and the circuit loop containing the specimen site. This expression includes the effects of all stray inductances and stray mutual inductances. We measure the value $M_{F\text{-}S}^{-1} = 460 \pm 10\ \mu\mathrm{A}/\Phi_0$, and from the geometry of the susceptometer chip we esti-

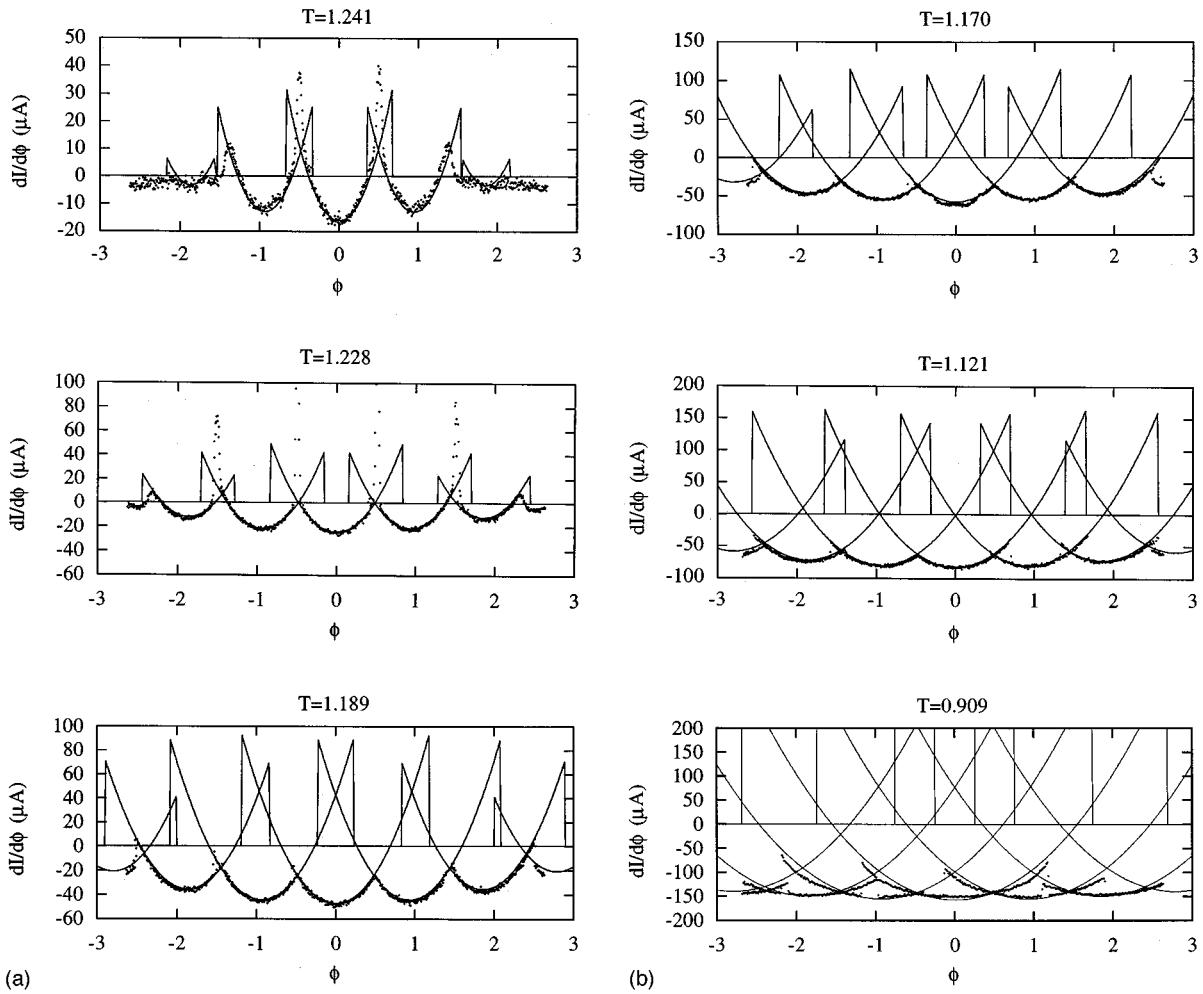


FIG. 4. Susceptibility of the aluminum ring at six temperatures plotted versus $\phi \equiv \Phi/\Phi_0$. The small dots are data as obtained directly from the lock-in amplifier shown in Fig. 3. No background subtraction or other processing of the data has been done. The solid lines are from the derivative of Eq. (12) with the four fit parameters of Eq. (15) and the calibration constants from Sec. II.

mate $M_F = 89 \pm 13$ pH. This gives the result $M_{R\text{-}S}^{-1} = 0.24 \pm 0.04$ A/$\Phi_0$. The uncertainty in this calibration factor is dominated by $M_F$ which we believe is known to about 15%, based on our ability to predict $M_{F\text{-}S}$ from model parameters.

### III. GINZBURG-LANDAU BEHAVIOR

In this section we present the susceptibility data for conditions where thermodynamic fluctuations are not important. The observations are compared to a Ginzburg-Landau theory for the ring. We use the results of the comparison between experiment and theory to measure certain parameters of the sample and to refine our values for other parameters. Because the sample parameters are important for what follows in later sections, we go into some detail here about how the parameters and their uncertainties are determined.

The data were collected with an ac flux amplitude of 0.05 $\Phi_0$, and the average applied flux was slowly swept from $-2.7\ \Phi_0$ to $+2.7\ \Phi_0$ and then back to $-2.7\ \Phi_0$. Our results for six temperatures are shown in Fig. 4. The data have been plotted using the values of the calibration constants $M_{F-R}$ and $M_{R-S}$ given in Sec. II above. In Fig. 5 we show the temperature dependence of the susceptibility at the periodic minima which occur at the flux values given by Eq. (1) for $n = 0, \pm 1, \pm 2$.

We next develop a Ginzburg-Landau theory for the data. The geometry of our ring is shown in Fig. 6. We the neglect effects of the self-field generated by the supercurrent and any radial variations of the order parameter. As we will discuss later, the validity of these approximations depends on the magnetic penetration depth $\lambda$ being greater than the thickness of the ring, and the Ginzburg-Landau coherence length $\xi$ being greater than the width of the ring.

The applied magnetic field is assumed to be uniform and perpendicular to the plane of the ring. It may be described by a vector potential

$$\vec{A} = \frac{1}{2} rB\hat{\theta}. \tag{3}$$

The order parameter without radial variations takes the form

$$\psi = fe^{in\theta} \quad n = \cdots -2, -1, 0, 1, 2, \ldots . \tag{4}$$

With these approximations, the Ginzburg-Landau free-energy density is given by

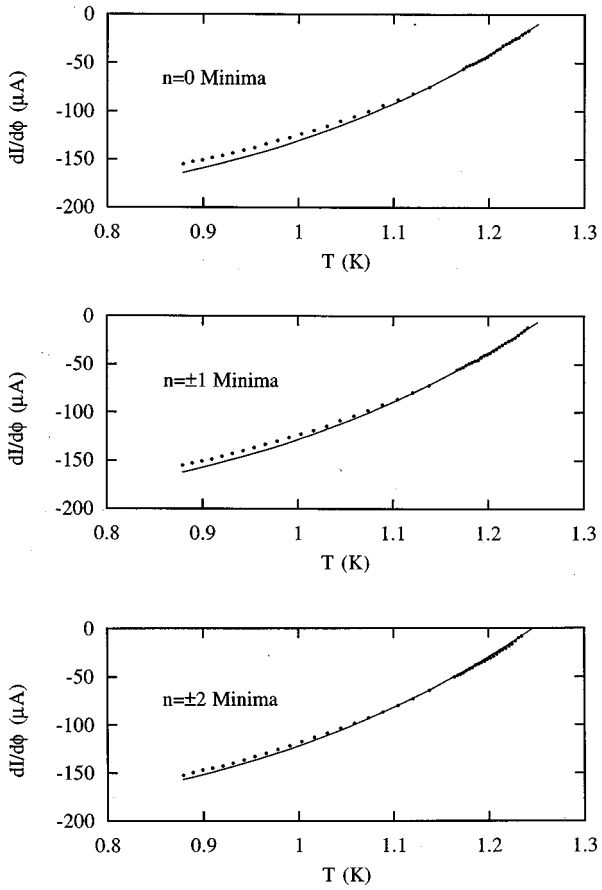


FIG. 5. The temperature dependence of the susceptibility at the minima corresponding to the solutions $n=0, \pm 1, \pm 2$. The solid line is from Eq. (12).

$$F/V=\alpha f^2+\frac{1}{2}\beta f^4+\frac{f^2}{2m^*V}\int_V\left(-\frac{n\hbar}{r}+\frac{1}{2}e^*rB\right)^2 d^3r. \tag{5}$$

By minimizing the free energy, we find an expression for the order-parameter amplitude

$$f^2=-\frac{\alpha}{\beta}-\frac{1}{\beta}\frac{\hbar^2}{4mR^2}\left\{\left(n-\frac{\Phi}{\Phi_0}\right)^2+\left[\frac{n^2}{3}+\left(\frac{\Phi}{\Phi_0}\right)^2\right]\left(\frac{w}{2R}\right)^2\right\}. \tag{6}$$

Here $R$ is the mean radius of the ring, $\Phi$ is the flux through the ring out to the mean radius, $\Phi_0$ is the flux quantum $(h/2e)$, and $w$ is the width of the ring. Only the terms of lowest order in the small parameter $w/2R$ have been retained. If the right side of Eq. (6) is negative, then $f^2=0$ and the system is in the normal state. By setting Eq. (6) equal to zero, a formula for the location of the mean-field phase boundary may obtained. This formula has been used to describe the Little-Parks $T_c$ oscillations.[6] The term containing $w/2R$ causes a suppression of the order parameter at high fields. It is clear from Fig. 4 that it is essential to include this aperiodic suppression to describe our data.

The thermodynamic current of the ring is given by the derivative

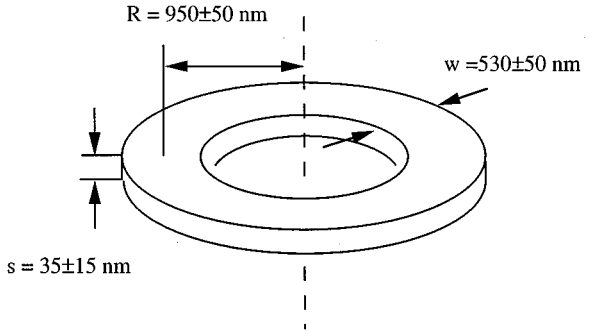


FIG. 6. Sample geometry and dimensions. These are the dimensions known independently from the susceptibility data. As discussed in the text, from the data the value for the thickness can be refined to $s=20\pm4$ nm.

$$I=-\frac{\partial F}{\partial\Phi}=-\frac{2V}{\Phi_0}\frac{\alpha}{\beta}\frac{\hbar^2}{4mR^2}\left\{n-\left[1+\left(\frac{w}{2R}\right)^2\right]\phi\right\}\times\left\{1+\frac{\hbar^2}{4mR^2\alpha}\left[(n-\phi)^2+\left(\frac{w}{2R}\right)^2\left(\frac{n^2}{3}+\phi^2\right)\right]\right\}, \tag{7}$$

where $\phi=\Phi/\Phi_0$, and $V$ is the sample volume. This is the equivalent current which, if concentrated at the mean radius $R$, would have the same energy of interaction with the applied field as the true current distribution.

To include the temperature dependence, we express the parameters $\alpha$ and $\beta$ in terms of the critical field $H_c$ and the magnetic penetration depth $\lambda$ using the standard relations[22]

$$-\frac{\alpha}{\beta}=\frac{m}{2\mu_0e^2\lambda^2}, \tag{8}$$

$$\frac{1}{\beta}=\frac{m^2}{4\mu_0^3e^4\lambda^4H_c^2}, \tag{9}$$

where $m$ and $e$ are the electron mass and charge. Then we insert phenomenological temperature dependences

$$H_c(T)=H_c(0)\left[1-\left(\frac{T}{T_c}\right)^2\right], \tag{10}$$

$$\frac{1}{\lambda^2(T)}=\frac{1}{\lambda^2(0)}\left[1-\left(\frac{T}{T_c}\right)^4\right]. \tag{11}$$

Substituting Eqs. (8)–(11) into Eq. (7) yields our final formula

$$I(\phi,t)=I_0A(1-t^4)(n-(1+\epsilon^2)\phi)\times\left\{1-\overline{\xi}^2\frac{1+t^2}{1-t^2}\left[(n-\phi)^2+\epsilon^2\left(\frac{n^2}{3}+\phi^2\right)\right]\right\}, \tag{12}$$

which is expressed in terms of the dimensionless temperature $t\equiv T/T_c$. The four parameters contained in Eq. (12) are

$$I_0=\frac{\Phi_0}{2\pi\mu_0R},\quad A=\frac{sw}{\lambda^2(0)},\quad \overline{\xi}=\frac{\xi(0)}{R},\quad \epsilon=\frac{w}{2R}, \tag{13}$$

where $s$ is the sample thickness, and $\xi(0)$ is the Ginzburg-Landau coherence length at zero temperature. In terms of the critical field and penetration depth the coherence length is

$$\xi(T)=\frac{\Phi_0}{\sqrt{8}\pi\mu_0 H_c(T)\lambda(T)}. \tag{14}$$

We next compare the data with the theory by fitting the parameters $I_0A$, $\xi$, $\epsilon$, and $T_c$, and then comparing the fit values with known sample parameters. The fit is done in a way which seeks exact agreement only in the limit $T\rightarrow T_c$. The best-fit parameter values obtained by fitting with Eq. (12) are

$$I_0A=200\pm 30\ \ \mu\text{A}, \quad \overline{\xi}=0.203\pm 0.006,$$
$$\epsilon=0.271\pm 0.008, \quad T_c=1.266\pm 0.003\ \ \text{K}. \tag{15}$$

The 15% uncertainty in the fit value of $I_0A$ accounts for the fact that this parameter is sensitive to the calibration constant $M_{R\text{-}S}$. The solid curves shown in Figs. 4 and 5 are obtained by plotting the derivative of Eq. (12) using the best-fit parameters. Equation (12) gives an excellent description of the data for temperatures above $t\approx 0.90$.

The mean-field critical temperature $T_c$ is defined as the point where the zero-field susceptibility shown in Fig. 5 extrapolates linearly to zero. Contributions to the fit value due to thermodynamic fluctuations are expected to be very small (see Sec. V). The fit value is somewhat higher than the bulk value of 1.175 K, as is often seen in thin aluminum films. The geometrical parameter $\epsilon$ obtained from the measured ring dimensions given in Fig. 6 is $\epsilon=0.279\pm 0.030$, in very good agreement with the fit value. The fit value of $\xi$ can be used to compute the product $\mu_0 H_c(0)\lambda(0)=12{,}000\pm 700$ G nm. This cannot be directly compared with any *a priori* value because $\lambda(0)$ (which depends on disorder) is not known. However, the value is very reasonable for evaporated aluminum films, and close to that measured by Groff and Parks.[6] By using the known critical field of aluminum of $H_c(0)=100$ Oe we may obtain $\lambda(0)=120\pm 7$ nm from the value of $\mu_0 H_c(0)\lambda(0)$ given above. Groff and Parks showed that values of $\lambda(0)$ measured in this way agree well with values deduced from transport data together with the theory of the dirty penetration depth.

The parameter $I_0A$ also depends on $\lambda(0)$, as well as known geometrical parameters. It can thus be used to find another independent value for the penetration depth. We find $\lambda(0)=160\pm 38$ nm, which is consistent with, but less accurate than, the previous value. Because the uncertainty is dominated by the ring thickness $s$, it is possible to use the previous more accurate value of $\lambda(0)$ to refine our value for the thickness. In this way we obtain $s=20\pm 4$ nm. This agreement between the two values of $\lambda(0)$ may be viewed as a check on our calibration constant $M_{R\text{-}S}$.

As mentioned earlier, we have neglected both self-field effects and radial variations of the order parameter. We expect the self-field effects to be small when $\lambda(T)\gg s$. For the data shown in this section $\lambda(T)$ is greater than 140 nm and so this condition is satisfied. We may also compare the self-flux induced by the supercurrent to the applied flux. For an estimate of the self-flux we use the formula for the self-inductance of an annulus with a uniform current distribution[23]

$$L=\mu_0 R\left[\ln\left(\frac{8R}{w}\right)-\frac{1}{2}\right]. \tag{16}$$

We find that the self-flux is not larger than 4% of the applied flux for $t>0.90$, but that it may be as large as 16% of the applied flux at the lowest temperature shown in Figs. 4 and 5. We can also compare the self-inductance energy $1/2\ LI^2$ to the condensation free energy of Eq. (5). The ratio of these quantities does not exceed 4% for any of the data shown. The one-dimensional form of the order parameter Eq. (4) is appropriate only if the Ginzburg-Landau coherence length $\xi(T)$ is much greater than the width of ring. This condition is always satisfied sufficiently close to $T_c$. For our parameters the coherence length becomes equal to the width at $t=0.88$. These estimates suggest that the departure of the theory from the data at the lowest temperatures may be due both to self-flux and to increasing radial dependence of the order parameter.

The solutions given by Eqs. (4) and (6) are local minima of the Ginzburg-Landau free energy for functions with uniformly varying phase. Additional analysis is needed to determine if these solutions are stable when small variations with nonuniform phase are considered.[18,24] The conclusion is that the solutions are only stable for flux values sufficiently close to the minimum points given by Eq. (1). In practice, thermal fluctuations allow phase slips well before the solutions become unstable. The $n=0$ to $n=1$ phase-slip transition will be discussed in detail in Sec. IV below.

The discussion thus far does not explain the sharp positive peaks seen in Fig. 4 at the two highest temperatures. These peaks do not represent the true static susceptibility, but are an artifact of our ac detection method. They occur when the $0.05\ \Phi_0$ amplitude ac applied flux causes repeated phase-slip transitions at the ac drive frequency. They disappear at lower temperatures where the free-energy barrier between adjacent states becomes too large to allow such repeated transitions. Although it is possible to give a quantitative analysis of these repeated transitions,[18] we prefer to analyze phase slips in the manner discussed in the next section, where the conditions are chosen to allow only a single transition.

## IV. THERMODYNAMIC FLUCTUATIONS: PHASE SLIPS

In this section we discuss the large fluctuations which cause transitions between different local minima of the free energy. Our results concern the $n=0$ to $n=1$ transition shown in Fig. 7. The transition rate is measured by first setting the dc flux to zero to place the ring in the $n=0$ state. Then the flux is swept quickly to a positive value where the $n=0$ state is metastable with a transition rate to the $n=1$ state in the range $10^0$–$10^{-4}$ $\text{s}^{-1}$. An $0.05\ \Phi_0$ amplitude ac flux at 1 kHz is continuously applied so that the susceptibility can be detected. When the susceptibility changes, indicating that the transition has occurred, the time delay is recorded and the flux is returned to zero. This process is repeated many times for each value of flux and temperature. The individual time delays appear to be drawn from a stationary process and can be fit to an exponential distribution.

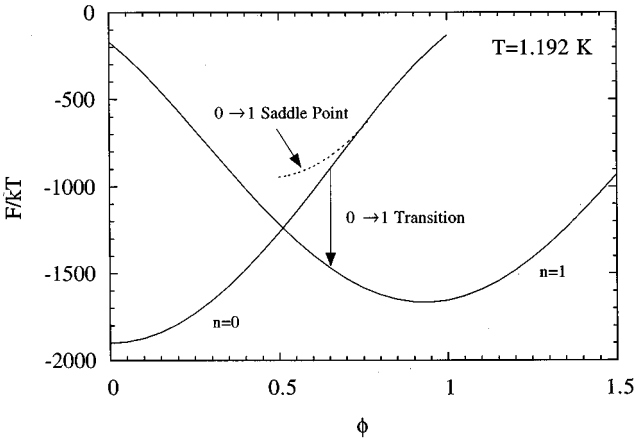


FIG. 7. Phase-slip transition from $n=0$ to $n=1$. The two solid lines are the free energies of the initial and final states. The dashed line is the free energy of the saddle point that must be traversed in the $n=0$ to $n=1$ transition. The $n=0$ solution becomes unstable at the value flux where the saddle-point energy meets the $n=0$ energy.

In this way the mean transition rates shown in Fig. 8 have been determined.

In Appendix B we present a theory for the transition rate following the calculation of Langer and Ambegaokar,[15] who discussed phase slips in superconducting wires which are one-dimensional with respect to the coherence length. The phase-slip rate is of the form

$$R \equiv \Omega \exp\left(-\frac{F_s - F_0}{kT}\right). \tag{17}$$

The barrier height $\Delta F \equiv F_s - F_0$ is the difference between the free energy $F_s$ of a saddle-point solution of the Ginzburg-Landau equations and the free energy $F_0$ of the initial ($n=0$) state. The saddle-point solution is the state of highest free energy between the initial and final states along the path in function space followed by the transition. It has the same phase winding number as the initial state (zero in this case),

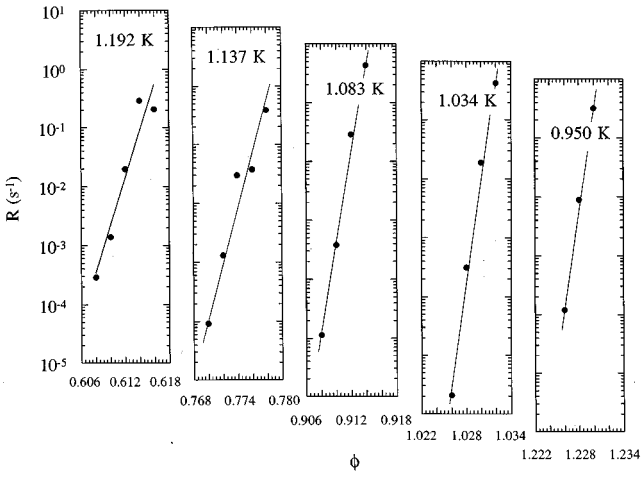


FIG. 8. Measured phase-slip rate as a function of flux for five different temperatures. The lines are a linear fit to the data. The measured rates are obtained by fitting to the exponentially distributed delay times observed at each value of flux and temperature.

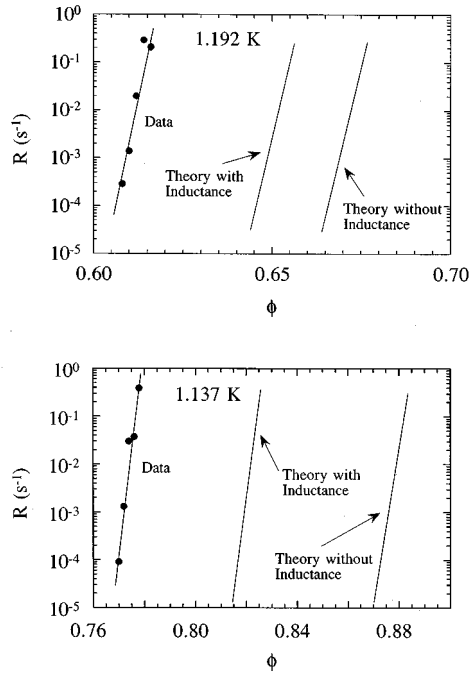


FIG. 9. Comparison of the measured phase-slip rate with predictions of theory. The curve labeled ''theory with inductance'' includes the effects of the self-inductance energy 1/2 $LI^2$.

but nonuniform amplitude and phase variations around the circumference. Our theory for the barrier height neglects self-field effects and radial variations of the order parameter, but includes first corrections for the width of the ring (the same approximations as were used in Sec. III above). For the prefactor $\Omega$ we use the theory of McCumber and Halperin for one-dimensional wires,[14,25] which gives

$$\Omega \approx \frac{2\pi R}{\xi}\sqrt{\frac{\Delta F}{kT}}\frac{1}{\tau}, \tag{18}$$

where $\tau$ is a relaxation time from the time-dependent Ginzburg-Landau equation

$$\tau = \frac{\pi h}{8k(T_c - T)}. \tag{19}$$

Our results are extremely insensitive to the value of the prefactor, and so we have not included refinements to the prefactor given by McCumber and Halperin, or recently derived corrections arising from the finite circumference.[26]

Figure 9 shows predictions of the theory for the highest two temperatures, for which our Ginzburg-Landau description is most accurate. Because the rate is a very rapid function of flux, it is important to average the theory over the ac variations of the flux. The average is strongly dominated by the highest flux values, so that to a good approximation the theory for the barrier height should be evaluated at the peak flux (the dc flux plus 0.05 $\Phi_0$). Both the predictions and the data in Fig. 9 are plotted as a function of the dc flux.

For the highest temperature the theory predicts switching at a dc flux value which is about 0.07 $\Phi_0$ too large. The magnitude of this discrepancy reflects only a very small error in the predicted saddle-point energy. To obtain a rate of 1 $s^{-1}$ requires a barrier height $\Delta F/kT$ of about 25. As can be seen

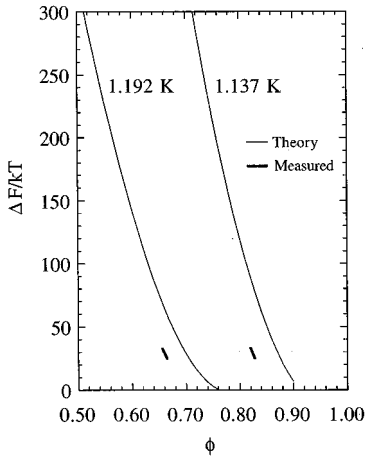


FIG. 10. Comparison of the measured free-energy barrier height with theory. The measured value is computed using the theoretical prefactor of Eq. (18). It is plotted at the flux value where the transition actually occurs, which is 0.05 $\Phi_0$ above the dc flux. The theoretical barrier height is computed using the theory of Appendix B with the self-inductance correction.

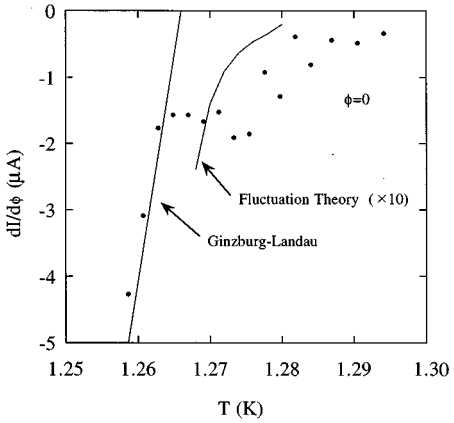


FIG. 11. The susceptibility at zero flux very close to the critical temperature. The curve labeled Ginzburg-Landau is from Eq. (12) with the four fit parameters of Eq. (15). The curve labeled Fluctuation Theory has been multiplied by 10 before being plotted. It is from Eqs. (20)–(22) which include the effects of thermodynamic fluctuations.

from Fig. 7, this is only 2.8% of the values of $F_0$ and $F_s$ individually. Thus the predicted rate depends on a very small difference between two nearly equal energies. Note also that with $\Delta F/kT=25$ an order of magnitude change of the prefactor $\Omega$ corresponds to only a 10% change in the barrier height, or a 0.25% change in the saddle-point energy. Thus a crude theory of the prefactor is adequate.

The various approximations in our theory are expected to cause slightly different errors for the saddle-point and $n=0$ energies. In particular, the currents of the two states differ and this will lead to different self-field corrections. For the curves labeled ''theory with inductance'' in Fig. 9 the self-inductance energy $1/2\,LI^2$ has been added to both the saddle-point and the initial-state energies, using Eq. (16) to estimate the self-inductance, and currents from Eq. (12) and Appendix B. At 1.192 K the self-inductance correction only changes the saddle-point and initial-state energies by 2.0 and 3.7 %, but this is sufficient to reduce the error in the predicted switching point to about 0.04 $\Phi_0$. This is not an exact treatment of the self-inductance correction both because Eq. (15) does not reflect the true current distribution and because we have not solved the Ginzburg-Landau equations with the self-inductance energy included.

It is perhaps more direct to use the measured transition rates and the theoretical prefactor Eq. (18) to compute a measured barrier height, and then to compare this with the prediction. This is done in Fig. 10. The predicted barrier height at 1.192 K is about a factor of 2 too large, which could be accounted for by a saddle-point energy which is 2.5 % too large. Uncertainties in the sample parameters alone cannot account for this error, because the main uncertainty is in an overall factor, which effects the saddle-point and uniform-state energy in the same way. However, the above estimates suggest that self-field effects may be important, and it is also possible that radial variations of the order parameter may be important. The present agreement seems to be as good as can be expected within the approximations we have made.

## V. THERMODYNAMIC FLUCTUATIONS: FLUCTUATION SUSCEPTIBILITY

In this section we present results for the susceptibility just above the mean-field critical temperature of 1.266 mK. Our data for the zero-flux susceptibility are shown in Fig. 11. The scatter in the data is due in part to the SQUID noise and in part to a background susceptibility signal which becomes evident at very small signal levels. The flux dependence of the susceptibility for several temperatures is shown in Fig. 12. Although the effect is near the limit of our resolution, there is clearly a symmetric signal present near zero flux. The signal is reproducible over different runs of the cryostat, and always disappears into the noise about 30 mK above the mean-field $T_c$. The data shown in Fig. 11 were not used for the fit to Ginzburg-Landau theory discussed in the previous section, but are in good agreement with that fit below $T_c$. The signal above $T_c$ cannot be explained by uncontrolled variations of the cryostat temperature. Our thermometry indicates that the cryostat temperature is stable to about 0.5 mK. The very rapid temperature dependence of the phase-slip rate reported in the previous section provides a second check on our temperature stability. Fluctuations larger than a few mK would lead to large variations of the rate which were not observed.

Recent theoretical interest in the fluctuation susceptibility of superconducting mesoscopic rings has grown out of efforts to understand the susceptibility of normal-metal mesoscopic rings. In a pioneering experiment on an array of $10^7$ mesoscopic copper rings, Lévy *et al.*[27] observed an $h/2e$-period persistent current. Ambegaokar and Eckern[28] then advanced a diagrammatic theory which invoked electron-electron interactions as a possible explanation of the data of Levy *et al.*, and extended their theory to include the behavior of superconducting rings above $T_c$.[29] von Oppen and Riedel[30] showed that the Ambegaokar and Eckern theory for superconductors above $T_c$ (and with $T_c$ greater than the correlation energy $E_c$) is equivalent to a theory of thermodynamic fluctuations of the Ginzburg-Landau free energy in Gaussian approximation, and gave improved self-consistent

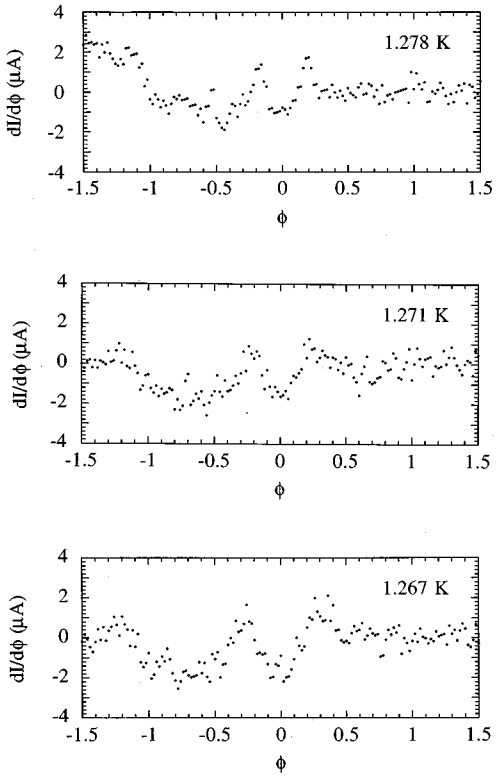


FIG. 12. The flux dependence of the susceptibility just above the mean-field critical temperature. This is a portion of the data used to construct Fig. 11. A linear background was subtracted from the data.

Hartree and Hartree-Fock results for the fluctuation susceptibility, which eliminated a divergence at $T_c$. von Oppen and Riedel also showed how the exact Ginzburg-Landau partition function for a one-dimensional ring can be recast as a two-dimensional quantum-mechanics problem, and gave essentially exact solutions for the fluctuation current by solving this new problem numerically.

In the Hartree-Fock approximation the von Oppen and Reidel result for the fluctuation current above $T_c$ is

$$I(\phi) = -\frac{2\pi kT}{\Phi_0} \frac{\sin(2\pi\phi)}{\cosh(2\pi y) - \cos(2\pi\phi)}, \tag{20}$$

where the self-consistency parameter $y$ is determined by

$$y^3 - \left(\frac{R}{\xi}\right)^2 y = \frac{1}{E_0}\left(\frac{R}{\xi}\right)^3 \frac{\sinh(2\pi y)}{\cosh(2\pi y) - \cos(2\pi\phi)}. \tag{21}$$

The dimensionless parameter $E_0$ is the condensation energy of one coherence length of the ring, in units of the critical temperature:

$$E_0 \equiv \frac{\mu_0 H_c^2}{kT_c}\, \xi s w. \tag{22}$$

The temperature dependence of these expressions is through the critical field $H_c(T)$ and the coherence length $\xi(T)$. This result is for a strictly one-dimensional ring and therefore it gives a periodic equilibrium current.

The zero-flux susceptibility obtained from the derivative of Eq. (20) is plotted in Fig. 11 (curve labeled Fluctuation Theory). The predicted susceptibility is a factor of 10–50 times smaller than the observed signal. Unlike the phase-slip rate, this prediction does not depend sensitively on the sample parameters. Uncertainties in the sample parameters or calibration factors cannot be used to significantly improve the agreement. We have extended the von Oppen and Reidel theory by averaging the free energy over the sample width (as was done in Sec. III above) to find corrections to lowest order in $w/2R$. We have also used the method of von Oppen and Reidel to go beyond the Hartree-Fock approximation and compute the exact one-dimensional susceptibility in this extended theory.[18] None of these efforts significantly improves the poor agreement between theory and experiment shown in Fig. 11. At the temperatures shown in Fig. 11, the coherence length is not less than 1.3 $\mu$m, and so there is no possibility that the equilibrium fluctuations excite radial modes which are not included in the one-dimensional theories. Despite the fact that the susceptibility of the ring below $T_c$ is described very well by the Ginzburg-Landau model of Sec. III, we conclude that this same model with thermodynamic fluctuations included is unable to describe the fluctuation susceptibility just above $T_c$.

It is conceivable that the effect we see will require an explanation involving novel physics. However, at least two conventional explanations should be considered first. One possibility is that our effect is due to fluctuations of the order parameter, but that these fluctuations are driven by external noise rather than by thermal fluctuations. In this case, modes of the order parameter could be excited more strongly and the fluctuation susceptibility could be larger than predicted by the equilibrium theory. One would have to hypothesize mean energies for fluctuating modes 10–50 times larger than in equilibrium. [As can be seen from Eq. (20), the equilibrium fluctuation current is proportional to the equipartition energy $kT$.] A detailed theory would depend on the spectrum of the fluctuating driving force, which might be different than in equilibrium. We do not favor an explanation along these lines for two reasons. First, we have not been able to identify a plausible source for the external noise. The source would have to couple strongly to the sample current without significantly heating the sample or other parts of the apparatus. The Josephson oscillations of the SQUID do not seem to be implicated because our signal does not depend upon the bias conditions of the SQUID. Second, the phase-slip data presented in the previous section show that the fluctuations of the order parameter below $T_c$ cannot be excited to energies more than about twice the ambient temperature.

Another possibility is that our description of the system as a homogeneous ring is not adequate very close to $T_c$. Perhaps variations in the ring material at different points around the circumference could lead to a smearing of the apparent critical temperature. We do not see any clear way to address this hypothesis with the results presented here. With data on many rings it might be possible to determine if the effect we see is sample specific, or if it depends on the microstructure of the material. If the effect were found to be sample independent and robust against changes in the microstructure, then an explanation based on inhomogeneity would not be tenable.

## VI. DISCUSSION

We conclude with a few remarks on previous experiments, and on the possible existence of a ''singly connected'' state. Vloeberghs *et al.*[31] have conducted transport experiments on 1 $\mu$m diameter aluminum rings with special attention to the Little-Parks oscillations of the critical temperature as a function of applied flux. They observed anomalous behavior, particularly at low fields, which is not consistent with an equilibrium Ginzburg-Landau description. The good agreement between our data and an equilibrium description indicates that the features observed by Vloeberghs *et al.* are almost certainly nonequilibrium effects. Indeed, the authors suggest that their effect may be related to a resistance enhancement above $T_c$ observed by Santhanam *et al.* in aluminum wires.[32] Experiments on the magnetization of a large array of 12 $\mu$m diameter indium disks in the vicinity of the 3.25 K superconducting critical temperature have been reported by Buisson *et al.*[33] An oscillation of the magnetization versus flux was observed, with an amplitude much less than was expected from a prediction based on Ginzburg-Landau theory. The authors suggested that this behavior may be due to degraded material near the outer radius of the disk which changes the effective boundary condition. Our data shows that no such modification of the boundary conditions occurs in small aluminum rings.

Several recent papers have argued that there exists a class of solutions to the Ginzburg-Landau equations for which the order parameter is zero at one point along the circumference.[24,34,35] Such solutions would trade the energy cost of suppressing the order parameter at a point for the energy gained by relaxing the fluxoid quantization constraint. Berger and Rubenstein[34] showed that in uniform one-dimensional rings such singly connected states are never global minima, but in a ring with small variations of the width they could become global minima in a small range of temperature and flux. Horane *et al.*[24] have argued that even in a uniform ring these solutions are local minima (for certain values of flux and temperature) and the system may linger in such a state while making a transition between uniform states. The singly connected state has zero circulating current, so a transition to such a state would cause the susceptibility to switch abruptly to zero. (For a ring of finite width, the susceptibility would be go to a small, but nonzero, value.) No such transitions to a state of near zero susceptibility were observed in the switching data used to produce Fig. 8. If the zero current state does exist, then its lifetime is less than about 1 s under our conditions.

The major puzzle presented by our results is the anomalously large susceptibility observed just above $T_c$. We do not have any explanation for this signal. We think that we have eliminated explanations based on uncertainties in the sample parameters, temperature fluctuations, and the possibility of a noise-driven effect. We have not ruled out the possibility that it could be caused by inhomogeneities in the ring. This could be addressed in future experiments which would compare the behavior of several nominally similar rings.

## ACKNOWLEDGMENTS

We would like to thank Michael Cromar and Martin Huber for help with the susceptometer device, and John Martinis and Rick Welty for the SQUID amplifier devices. We wish to thank Sihan Lin, Art Klittnick, Jinzhong Pang, James Mooney, and Patrick Sullivan for their assistance. We are grateful for discussions with Daniel Reich and Dragomir Davidovic. This work was supported by the Office of Naval Research under N00014-90-J-1891, the National Science Foundation under DMR-9057426, and the David and Lucile Packard Foundation.

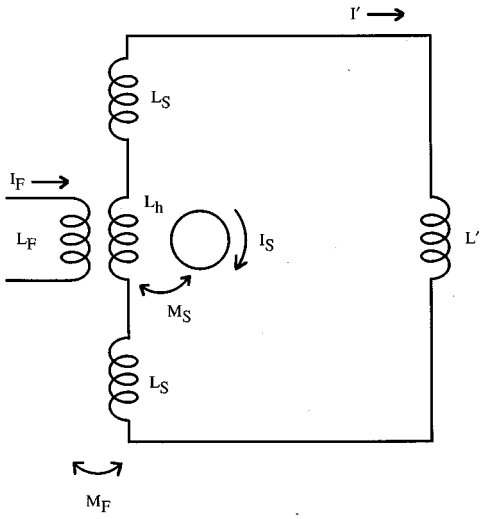


FIG. 13. Circuit model of the susceptometer device.

## APPENDIX A: CALIBRATION CONSTANT $M_{R\text{-}S}$

The calibration constant $M_{R\text{-}S}$ is defined as the ratio of the flux induced in the input SQUID loop to the sample current, with zero field current. It can be expressed in terms of a minimum number of model parameters with the help of Fig. 13.

The field coil inductance $L_F$ is coupled through the mutual inductance $M_F$ to the specimen site or sample hole inductance $L_h$. The inductances $L_S$ represent strays in the immediate vicinity of the specimen site due to the spreading of current at the corners of the hole. Because the field coil is wrapped around both the specimen site and these strays, the mutual inductance $M_F$ is given by $M_F = n_F(L_h + 2L_S)$, where $n_F$ is the number of turns in the field coil. The sample ring is coupled to the specimen site through the mutual inductance $M_S$. The current $I_F$ is the current in the field coil, and the current $I_S$ is the sample current. The effective inductance $L'$ represents the total inductance seen by the sample site, which includes the inductance of the other 4 $\mu$m hole, the transformer primary, the SQUID inductance coupled through the matching transformer, and various additional strays. The SQUID flux $\Phi_S$ due to the field current or sample current is proportional to the loop current $I'$ (see Fig. 13), and we will express it as $\Phi_S = \alpha L' I'$, where $\alpha$ is a dimensionless coupling constant.

The ratio of the SQUID flux to the unbalanced field coil current (in the absence of a sample) is then given by

$$M_{F\text{-}S} = M_F \frac{L'}{L' + L_h + 2L_S} \alpha, \tag{A1}$$

and similarly the ratio of the SQUID flux to the sample current is

$$M_{R\text{-}S}=M_S\,\frac{L'}{L'+L_h+2L_S}\,\alpha. \tag{A2}$$

The final quantity we need is $M_{F\text{-}R}$, the ratio of the flux applied to the sample to a balanced field coil current (in the absence of any induced sample currents). In this case the current $I'$ is zero, so the flux in $L_h$ is $n_F L_h I_F$. The fraction of the flux in $L_h$ which goes through the sample is the flux in $L_h$ multiplied by the ratio $M_S/L_h$. Thus we find $M_{F\text{-}R}=n_F M_S$. Substituting this result and Eq. (A1) into Eq. (A2) gives Eq. (2) of the main text.

## APPENDIX B: THEORY OF PHASE-SLIP RATE

The mean-field order parameters of the form $f\exp(\mathrm{in}\theta)$ derived in Sec. III have uniform magnitude and uniformly varying phase. Each solution represents a local minimum of the free energy [for flux values close enough to the minimum points of Eq. (1)]. If there were no thermal fluctuations, these solutions would be perfectly stable. Langer and Ambegaokar[15] found the saddle point on the path through function space between two uniform solutions with different values of $n$. The energy of this saddle-point solution determines the phase-slip transition rate. Their theory was in strict one dimension and for an infinitely long wire. We extend the theory to a ring of finite circumference in a magnetic field, and we include first corrections for the width of the ring (see also Ref. 26). As in Sec. III, both self-field effects and radial variations of the order parameter are neglected.

At a saddle point the free energy is stationary with respect to small changes in $\Psi$, so that $\Psi$ should satisfy the Ginzburg-Landau equations,

$$\alpha\overline{\psi}+\beta|\overline{\psi}|^2\overline{\psi}+\frac{\hbar^2}{2m^*}\left(-i\nabla-\frac{e^*A}{\hbar}\right)^2\overline{\psi}=0. \tag{B1}$$

We look for solutions of the form

$$\overline{\psi}=f(\theta)\exp[i\chi(\theta)]. \tag{B2}$$

The equations then become

$$\alpha f+\beta f^3+\frac{\hbar^2}{2m^*}\left[f\left(\frac{1}{r}\frac{d\chi}{d\theta}-\frac{e^*A}{\hbar}\right)^2-\frac{1}{r^2}\frac{d^2f}{d\theta^2}\right]=0,$$

$$\frac{1}{rf}\frac{d}{d\theta}\left[f^2\left(\frac{1}{r}\frac{d\chi}{d\theta}-\frac{e^*A}{\hbar}\right)\right]=0. \tag{B3}$$

The second of these equations shows that the current density,

$$\mathbf{J}(r)=\frac{\hbar e}{m}\,f^2\left(\frac{1}{r}\frac{d\chi}{d\theta}-\frac{e^*A}{\hbar}\right)=\frac{\hbar e}{m}\,J(r), \tag{B4}$$

only depends on the radius. With the substitutions

$$\alpha''=\frac{2m^*|\alpha|}{\hbar^2},\quad \beta''=\frac{2m^*}{\hbar^2}\,\beta, \tag{B5}$$

we obtain

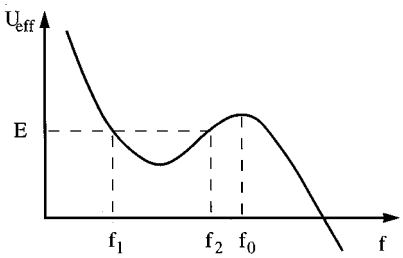


FIG. 14. Effective radial potential for the magnitude of the order parameter.

$$-\alpha''f+\beta''f^3+\frac{J^2(r)}{f^3}-\frac{1}{r^2}\frac{d^2f}{d\theta^2}=0. \tag{B6}$$

This obviously has no exact solutions since $f$ does not depend on $r$. Approximate solutions which include the effects of the finite width can be obtained by averaging over the radius, the same procedure we followed in Sec. III for the uniform solutions. The result is

$$-\alpha''f+\beta''f^3+\frac{\langle J^2\rangle}{f^3}-\frac{1}{2\epsilon}\ln\left[\frac{1+\epsilon}{1-\epsilon}\right]\frac{1}{R^2}\frac{d^2f}{d\theta^2}=0, \tag{B7}$$

where as before $\epsilon=w/2R$, a small parameter. Now let $\alpha'=\alpha''/\epsilon'$, $\beta'=\beta''/\epsilon'$, $J'^2=\langle J^2\rangle/\epsilon'$ and $x=R\theta$, where $\epsilon'=1/2\epsilon\ln[(1+\epsilon)/(1-\epsilon)]$. Equation (B7) then becomes

$$-\alpha' f+\beta' f^3+\frac{J'^2}{f^3}-\frac{d^2f}{dx^2}=0. \tag{B8}$$

Equation (B8) is of the same form as found by Langer and Ambegaokar, and it may be solved by the same method, although our case is somewhat more involved because of the boundary conditions. It may be interpreted as the equation of motion of a particle moving in an effective radial potential

$$\frac{d^2f}{dx^2}=-\frac{d}{df}\left[\frac{J'^2}{2f^2}+\frac{1}{2}\,\alpha' f^2-\frac{1}{4}\,\beta' f^4\right]=-\frac{d}{df}\,U_{\mathrm{eff}} \tag{B9}$$

with $f$ as the radial coordinate and $x$ playing the role of time. The conservation of total energy $E$ reads

$$\frac{d}{dx}\left[\frac{1}{2}\left(\frac{df}{dx}\right)^2+U_{\mathrm{eff}}(f)\right]\equiv\frac{dE}{dx}=0, \tag{B10}$$

or in integral form

$$x=\int_{f_1}^{f}\frac{df}{\sqrt{2[E-U_{\mathrm{eff}}(f)]}}, \tag{B11}$$

where we have chosen $f=f_1$ at $x=0$. The effective potential appears as in Fig. 14 for $J'$ not too large. Periodic motions which have a chance to satisfy the boundary conditions occur for $E<U_{\mathrm{eff}}(f_0)$. The turning points $f_1$ and $f_2$ satisfy $E=U_{\mathrm{eff}}(f_1)=U_{\mathrm{eff}}(f_2)<U_{\mathrm{eff}}(f_0)$. A solution may be selected by choosing either $E$ and $J'$ or $f_1$ and $f_2$, but only special choices will give $f$ and $\chi$ the correct periodicity.

Following Langer and Ambegaokar we introduce the dimensionless quantities

$$f^2=\frac{\alpha'}{\beta'}\,u,\quad J'=\sqrt{\frac{4\alpha'^3}{27\beta'^2}}\,j',\quad E=\frac{\alpha'^2}{2\beta'}\,\mathcal{E},\tag{B12}$$

and rewrite Eq. (B11) as

$$x=\frac{1}{\sqrt{2\alpha'}}\int_{u_1}^{u}\frac{du}{\sqrt{u^3-2u^2+2\mathcal{E}u-\frac{8}{27}j'^2}}.\tag{B13}$$

The cubic in the denominator can be factored

$$u^3-2u^2+2\mathcal{E}u-\frac{8}{27}j'^2=(u-u_0)(u-u_1)(u-u_2),\tag{B14}$$

and since the denominator is zero at the turning points we can identify

$$f_1^2=\frac{\alpha'}{\beta'}\,u_1,\quad f_2^2=\frac{\alpha'}{\beta'}\,u_2.\tag{B15}$$

Comparing the coefficients before the same power of $u$ yields

$$\begin{aligned}u_0+u_1+u_2&=2,\\ u_0u_1+u_0u_2+u_1u_2&=2\mathcal{E},\\ u_0u_1u_2&=\frac{8}{27}j'^2.\end{aligned}\tag{B16}$$

We will find that it is simplest to impose the boundary conditions in terms of new parameters $\Delta\equiv u_0-u_1$ and $y\equiv(u_2-u_1)/\Delta$. These are related to the $u$'s by

$$\begin{aligned}u_0&=\frac{2+(2-y)\Delta}{3},\\ u_1&=\frac{2-(1+y)\Delta}{3},\\ u_2&=\frac{2+(2y-1)\Delta}{3}.\end{aligned}\tag{B17}$$

Expressing the denominator in Eq. (B13) in terms of $u_1$, $u_2$ and $u_0$, we get the solution

$$\begin{aligned}x&=\frac{1}{\sqrt{2\alpha'}}\int_{u_1}^{u}\frac{du}{\sqrt{(u-u_0)(u-u_1)(u-u_2)}}\\ &=\frac{1}{\sqrt{2\alpha'}}\,\frac{2}{\sqrt{u_0-u_1}}\,F(\gamma,q),\end{aligned}\tag{B18}$$

where $F(\gamma,q)$ is an elliptic function of the first kind and

$$\gamma=\sin^{-1}\sqrt{\frac{u-u_1}{u_2-u_1}},\quad q=\sqrt{\frac{u_2-u_1}{u_0-u_1}}=\sqrt{y}.\tag{B19}$$

Two equations will be needed to determine $\Delta$ and $y$. A first relation can be found by requiring that $\theta=\pi$ at the turning point $f_2$, or equivalently that $x=\pi R$ at $u=u_2$. Equation (B18) then yields

$$\pi R=\frac{1}{\sqrt{2\alpha'}}\,\frac{2}{\sqrt{\Delta}}\,F\left(\frac{\pi}{2},\sqrt{y}\right).\tag{B20}$$

A second equation can be found by requiring that the phase be periodic modulo $2\pi$. To impose this condition we return to Eq. (B4) for the current

$$J^2=f^4\left(\frac{1}{r}\frac{d\varphi}{d\theta}-\frac{e^*A}{\hbar}\right)^2.\tag{B21}$$

Averaging over the width of the ring gives

$$\langle J^2\rangle/\epsilon'=J'^2=f^4\left[\left(\frac{d\chi}{dx}-\frac{1}{\epsilon'}\frac{\phi}{R}\right)^2+\frac{\epsilon''}{\epsilon'}\left(\frac{\phi}{R}\right)^2\right],\tag{B22}$$

where $\epsilon''=(1+\epsilon^2)-1/\epsilon'$. This can be solved for $d\chi/dx$ and integrated around the ring to find the total phase change. Imposing periodicity then yields

$$2\pi n=2\pi\,\frac{\phi}{\epsilon'}+2\int_0^{\pi R}\sqrt{\frac{J'^2}{f^4}-\frac{\epsilon''}{\epsilon'}\left(\frac{\phi}{R}\right)^2}\,dx.\tag{B23}$$

The integral can be evaluated approximately by expanding the square root to first or higher order in the small parameter $\epsilon''/\epsilon'$, which is proportional to $\epsilon^2$ when $\epsilon$ is small. Using the measure

$$du=\sqrt{2\alpha'}\sqrt{(u-u_0)(u-u_1)(u-u_2)}\,dx,\tag{B24}$$

each term can be then expressed in terms of elliptic functions of the first, second, or third kinds. With the square root expanded to first order we find

$$2\pi n\epsilon'=2\pi\varphi+\frac{2\sqrt{2}}{3\sqrt{3}}\,\epsilon' j' U_{-1}-\frac{3\sqrt{3}}{2\sqrt{2}}\,\frac{\varphi^2}{\alpha' R^2}\,\epsilon''\,\frac{1}{j'}\,U_{+1},\tag{B25}$$

where

$$\begin{aligned}\int_0^{\pi R}u\,dx&=\frac{1}{\sqrt{2\alpha'}}\,U_{+1}\\ &=\frac{1}{\sqrt{2\alpha'}}\left[\frac{2u_0}{\sqrt{\Delta}}\,F\left(\frac{\pi}{2},\sqrt{y}\right)-2\sqrt{\Delta}E\left(\frac{\pi}{2},\sqrt{y}\right)\right]\end{aligned}\tag{B26}$$

and

$$\int_0^{\pi R}\frac{1}{u}\,dx=\frac{1}{\sqrt{2\alpha'}}\,U_{-1}=\frac{1}{\sqrt{2\alpha'}}\,\frac{2}{u_1\sqrt{\Delta}}\,\Pi\left(\frac{\pi}{2},-\frac{y\Delta}{u_1},\sqrt{y}\right).\tag{B27}$$

This result gives a second relation between $\Delta$ and $y$ which completely specifies the solution. The results given in the main text were obtained by expanding the square root to second order, which leads to lengthy expressions.

We still need to find a result for the free energy of the saddle-point solution. The calculation proceeds as follows:

$$\overline{F}=\int d^3r\left[\alpha|\overline{\psi}|^2+\frac{1}{2}\beta|\overline{\psi}|^4+\frac{\hbar^2}{2m^*}\left|\left(-i\nabla-\frac{e^*\overline{A}}{\hbar}\right)\overline{\psi}\right|^2\right],$$

$$=-\frac{1}{2}\beta\int_V d^3r|\overline{\psi}|^4=-\frac{1}{2}\beta ws\int_{-\pi R}^{\pi R}dx f^4,$$

$$=-\frac{\alpha^2}{2\beta}ws\int_{-\pi R}^{\pi R}dx u^2, \tag{B28}$$

$$=-\frac{\alpha^2}{\beta}ws\frac{1}{\sqrt{2\alpha'}}\int_{u_1}^{u_2}\frac{u^2du}{\sqrt{(u-u_0)(u-u_1)(u-u_2)}},$$

$$=-\frac{\alpha^2}{\beta}ws\frac{1}{\sqrt{2\alpha'}}\left\{-\frac{2}{3}\sqrt{\Delta}\left[(2-y)\Delta E\left(\frac{\pi}{2},\sqrt{y}\right)-2\Delta(1-y)F\left(\frac{\pi}{2},\sqrt{y}\right)\right]\right.$$

$$\left.+2\sqrt{\Delta}(u_1+u_2)\left[F\left(\frac{\pi}{2},\sqrt{y}\right)-E\left(\frac{\pi}{2},\sqrt{y}\right)\right]+\frac{2u_1^2}{\sqrt{\Delta}}F\left(\frac{\pi}{2},\sqrt{y}\right)\right\}.$$

Barrier heights computed from this formula are shown in Figs. 7 and 10.


[1] B. S. Deaver and W. M. Fairbank, Phys. Rev. Lett. **7**, 43 (1961); R. Doll and M. Näbauer, *ibid.* **7**, 51 (1961).

[2] L. D. Jackel, W. W. Webb, J. E. Lukens, and S. S. Pei, Phys. Rev. B **9**, 115 (1974).

[3] L. D. Jackel, R. A. Buhrman, and W. W. Webb, Phys. Rev. B **9**, 115 (1974).

[4] R. Rouse, Siyuan Han, and J. E. Lukens, Phys. Rev. Lett. **75**, 1614 (1995).

[5] R. D. Parks and W. A. Little, Phys. Rev. **133**, A97 (1964).

[6] R. P. Groff and R. D. Parks, Phys. Rev. **176**, 567 (1968).

[7] J. M. Gordon, Phys. Rev. B **30**, 6770 (1984); M. Gijs, C. Van Haesendonck, and Y. Bruynseraede, *ibid.* **30**, 2964 (1984).

[8] N. E. Israelof, F. Yu, A. M. Goldman, and R. Bojko, Phys. Rev. Lett. **71**, 2130 (1993).

[9] A. Dimoulas *et al.*, Phys. Rev. Lett. **74**, 602 (1995); V. T. Petrashov, V. N. Antonov, P. Delsing, and T. Claeson, JETP Lett. **60**, 589 (1995).

[10] D. Davidovic *et al.*, Phys. Rev. Lett. **76**, 815 (1996).

[11] E. N. Bogachek, G. A. Gogadze, and I. O. Kulik, Phys. Status Solidi B **67**, 287 (1975).

[12] V. Chandrasekhar *et al.*, Phys. Rev. Lett. **67**, 3578 (1991); D. Mailly, C. Chapelier, and A. Benoit, *ibid.* **70**, 2020 (1993).

[13] Sean Washburn and Richard A. Webb, Adv. Phys. **35**, 412 (1986).

[14] W. J. Skocpol and M. Tinkham, Rep. Prog. Phys. **38**, 1049 (1975).

[15] J. S. Langer and Vinay Ambegaokar, Phys. Rev. **164**, 498 (1967); W. A. Little, *ibid.* **156**, 396 (1967).

[16] See R. S. Newbauer, M. R. Beasley, and M. Tinkham, Phys. Rev. B **5**, 864 (1972).

[17] R. A. Buhrman and W. P. Halperin, Phys. Rev. Lett. **30**, 692 (1973).

[18] Xiaxian Zhang, Ph.D. thesis, University of Colorado, 1996.

[19] J. M. Jaycox and M. B. Ketchen, IEEE Trans. Mag. **MAG-17**, 400 (1981).

[20] Suitable wire is manufactured by Tanaka Denshi Kogyo, 8-5-1 Simorenjaku, Mitaka-shi, Tokyo 181 [0422 (46) 8511]. U.S. liaison office, Santa Clara, CA [(408) 241-1630].

[21] R. P. Welty and J. M. Martinis, IEEE Trans. Appl. Supercond. **3**, 2605 (1993); IEEE Trans. Magn. **27**, 2924 (1990).

[22] Michael Tinkham, *Introduction to Superconductivity*, 2nd ed. (McGraw-Hill, New York, 1996).

[23] Frederick W. Grover, *Inductance Calculations* (Instrument Society of America, Research Triangle Park, 1973), p. 143.

[24] Emilio M. Horane, J. I. Castro, Gustavo C. Buscaglia, and A. Lopez, Phys. Rev. B **53**, 9296 (1996).

[25] D. E. McCumber and B. I. Halperin, Phys. Rev. B **1**, 1054 (1970).

[26] Martin B. Tarlie, Efrat Shimshoni, and Paul M. Goldbart, Phys. Rev. B **49**, 494 (1994).

[27] L. P. Lévy, G. Dolan, J. Dunsmuir, and H. Bouchiat, Phys. Rev. Lett. **64**, 2074 (1990).

[28] Vinay Ambegaokar and Ulrich Eckern, Phys. Rev. Lett. **65**, 381 (1990); Ulrich Eckern, Z. Phys. B **82**, 393 (1991).

[29] V. Ambegaokar and U. Eckern, Europhys. Lett. **13**, 733 (1990); Phys. Rev. B **44**, 10 358 (1991).

[30] Felix von Oppen and Eberhard K. Riedel, Phys. Rev. B **46**, 3203 (1992).

[31] H. Vloeberghs *et al.*, Phys. Rev. Lett. **69**, 1268 (1992).

[32] P. Santhanam *et al.*, Phys. Rev. Lett. **66**, 2254 (1991).

[33] Buisson *et al.*, Phys. Lett. A **150**, 36 (1990).

[34] Jorge Berger and Jacob Rubenstein, Phys. Rev. Lett. **75**, 320 (1995).

[35] D. Davidovic *et al.* (unpublished).